Spectroscopy of ^{7}He states using the (^{15}N,^{17}F) reaction on ^{9}Be

H. G. Bohlen,[1] R. Kalpakchieva,[2] A. Blaževi ć,[1,*] B. Gebauer,[1] T. N. Massey,[3] W. von Oertzen,[1,†] and S. Thummerer[1]
[1]*Hahn-Meitner-Institut GmbH, Glienicker Straße 100, D-14109 Berlin, Germany*
[2]*Flerov Laboratory of Nuclear Reactions, Joint Institute for Nuclear Research, Ru-141980 Dubna, Russia and Institute for Nuclear Research and Nuclear Energy, Bulgarian Academy of Sciences, 1784 Sofia, Bulgaria*
[3]*Department of Physics and Astronomy, Ohio University, Athens, Ohio 45701-2979*
(Received 10 February 2001; published 10 July 2001)

We have studied states of ^{7}He using the ^{9}Be(^{15}N,^{17}F)^{7}He reaction at two incident energies, $E_{lab}=240$ MeV and 318.5 MeV and observed clearly the first excited state of ^{7}He. An extended study of the three-body background was required to determine the excitation energy and width. The resonance parameters obtained for $l=1$ are $E_x=2.95(10)$ MeV, and $\Gamma=1.9(3)$ MeV. There is also evidence of a broad excited state at $E_x=5.8(3)$ MeV with $\Gamma=4(1)$ MeV. From the analysis of the ^{7}He ground state resonance, we extracted a value of 0.14(2) MeV for the width. In the calibration reaction ^{12}C(^{15}N, ^{17}F)^{10}Be three high-lying states of ^{10}Be are found at 13.6(1), 15.3(2), and 16.9(2) MeV.

DOI: 10.1103/PhysRevC.64.024312 PACS number(s): 21.10.Dr, 21.10.Pc, 25.70.Hi, 27.20.+n

I. INTRODUCTION

The ground state of ^{7}He is known from the work of Stokes and Young (1967) [1]. They used the ^{7}Li(t,^{3}He) reaction and found that the ground state is particle unstable with respect to the decay into ^{6}He+n by 0.44(3) MeV and has a width of 0.16(3) MeV. However, no excited states were found.

The observation of excited states of ^{7}He was a long standing question in nuclear spectroscopy although many attempts have been made to answer this question [2–7]. The difficulties in measuring the properties of an excited state of ^{7}He arise from the usual three-body background present in the measurement. Since ^{7}He is neutron unstable, transfer reactions like ^{9}Be(^{6}Li, ^{8}B) [2] or the pion absorption reaction ^{7}Li(π^{-},γ)^{7}He [4] always produce a continuous three-body background in addition to the population of ^{7}He resonances. The three particles in the exit channel are in this case ^{6}He $+n+$ outgoing particle (or γ ray), where the recoil nucleus ^{6}He may be either in the ground state or in the 2^{+} excited state at 1.80 MeV. Identification of small and broad resonances on such a background is difficult. Thus, a good description of the background and good statistics in the spectrum are required for a successful analysis.

Until 1998 the available data have only shown that no strong *narrow* resonance ($\Gamma<0.8$ MeV) exists in ^{7}He above the ground state up to at least 10 MeV excitation energy. Results on heavier helium isotopes show several excited states. For example, for the particle unstable isotope ^{9}He three to four states with a width smaller than 0.8 MeV have been found [5,8–10]. The structure of ^{7}He seems to resemble more ^{5}He in this respect (see, e.g., the analysis of Csóto and Hale [11] for ^{5}He).

A considerable number of structure calculations have been published on ^{7}He in the last decade. Shell model calculations [12,13] predict several excited states of ^{7}He: In the $(0+1)\hbar\omega$ model space low-lying states result at 2.26 MeV ($1/2^{+}$), 3.00 MeV ($1/2^{-}$), 4.88 MeV ($5/2^{-}$), 6.03 MeV ($5/2^{+}$), and in the $(0+2)\hbar\omega$ model space at 2.49 MeV ($1/2^{-}$), 3.52 MeV ($5/2^{-}$), 4.68 MeV ($3/2^{-}$).

Wurzer and Hofmann (1997) [14] predicted in the refined resonating group model two excited states: (1) $1/2^{-}$ in the range $E_x=2.3-3.8$ MeV, $\Gamma=3.6-5.4$ MeV, and (2) $5/2^{-}$ in the range $E_x=4.1-5.5$ MeV, $\Gamma=3.5-5.9$ MeV, depending on the background phase shifts of the hard sphere scattering (see [14]). The second state ($5/2^{-}$) is described by coupling a $1p1/2$ neutron to the excited 2^{+} state of the ^{6}He core. The corresponding $3/2^{-}$ coupling partner as well as $1d5/2$ and $2s1/2$ neutrons show no resonant behavior in this calculation.

Further structure calculations on ^{7}He have been published by Pudliner *et al.* (1997) [15] using quantum Monte Carlo calculations, and by Navrátil and Barrett (1998) [16] based on a large shell-model basis ($6\hbar\omega$). In the latter case very similar results as in the work of Wolters *et al.* [12] have been obtained with only slightly lower excitation energies.

We observed in the ^{9}Be(^{15}N,^{17}F)^{7}He reaction at 240 MeV, with strong evidence, an excited state of ^{7}He at about 3 MeV excitation energy, the preliminary results have been published in Ref. [17].

Recently Korsheninnikov *et al.* [18] found an excited state of ^{7}He at 2.9(3) MeV, with a width of 2.2(3) MeV, using the p(^{8}He,d)^{7}He reaction at 50 MeV/nucleon. The authors measured also in coincidence with the outgoing deuteron the decay particles ^{6}He or, ^{4}He emitted from the ^{7}He excited state, respectively, and deduced from the decay properties of the resonance a probable spin-parity assignment of $5/2^{-}$. A very recent publication [19] reports the observation of a structure in the tail of the ground state resonance at the high excitation energy side, which is interpreted as a further resonance of ^{7}He. The authors suggest that this is the $1/2^{-}$ spin-orbit partner of the ground state. The deduced resonance parameters are $E_R=1.2(2)$ MeV [$E_x=0.8(2)$ MeV], and

*Present address: TU Darmstadt, Darmstadt, Germany.
†Also at Fachbereich Physik, Freie Universität Berlin, Berlin, Germany.

$\Gamma_R = 1.0(2)$ MeV. However, this state has not been observed in the spectrum of relative velocities between ^{6}He and the neutron measured in an aligned configuration at $\theta_{lab} = 0°$ after fragmentation of ^{18}O on ^{9}Be at 80 MeV/nucleon [20], where it should also be present.

The paper has been organized as follows. After this introduction the details of the measurements and experimental setup are discussed in Sec. II. The description of the background, needed for the analysis is covered in Sec. III. The results of the analysis and the discussion of these results is presented in Sec. IV. The concluding remarks are given in Sec. V.

II. MEASUREMENTS

The two-proton pickup reaction ^{9}Be(^{15}N, ^{17}F)^{7}He has been measured at two incident energies, $E_{lab} = 240$ MeV and 318.5 MeV. The reaction has a ground state Q value of $Q_0 = -16.613$ MeV. The measurements have been performed at HMI with the Q3D magnetic spectrograph with an angular setting of $\theta_{Q3D} = 4°$ and with the aperture acceptance of $2.0° < \theta_{lab} < 5.3°$. The reaction products were identified by the focal plane detector using the energy loss in a gas-filled chamber and both the time of flight and the light output of a scintillator behind it. The position in the focal plane was measured using the delay-line read-out technique. For corrections of the kinematics on different target masses it was important to measure the precise scattering angle within the horizontal aperture opening of 3.3° (Fig. 1). The angle was deduced from the measured time of flight, since the trajectory length within the Q3D spectrograph depends on the angle. An angular resolution of 0.3° was achieved. A self-supporting ^{9}Be target with a thickness of 260 μg/cm^2 was used in the initial experiment, and of 450 μg/cm^2 in the later experiments. In order to determine the background for the ^{12}C and ^{16}O contents of the target (which in our case were low), we performed separate measurements on a ^{12}C and a V_2O_5 target, both with a thickness of 200 μg/cm^2, with identical field settings as for ^{9}Be. The ^{12}C(^{15}N, ^{17}F)^{10}Be reaction has also been used for the $B\rho$ calibration using only the central part of the angular aperture to eliminate kinematical effects.

In Fig. 1 an enhanced counting rate parallel to the ^{7}He ground state at about 2.9 MeV excitation energy can be seen; this indicates an excited state of ^{7}He as will be shown later. Projection of the two-dimensional spectra on the position axis resulted in momentum spectra with kinematical correction optimized for ^{9}Be target nuclei, but with some kinematical broadening for ^{12}C and ^{16}O target nuclei.

The latter spectra are only used to describe the corresponding background contribution in the spectrum of the ^{9}Be target. However, the good angular resolution allows an off-line kinematical correction also for the ^{12}C and ^{16}O targets, these spectra are shown in Figs. 2(c) and (d), together with the spectrum on ^{9}Be [panel (b)]. An energy resolution of 0.3 MeV was achieved. We have remeasured this reaction with much better statistics using a ^{9}Be-target of 450 μg/cm^2 thickness. The corresponding spectrum is shown in Fig. 2(a), it confirms with lower resolution (0.6 MeV) the previously

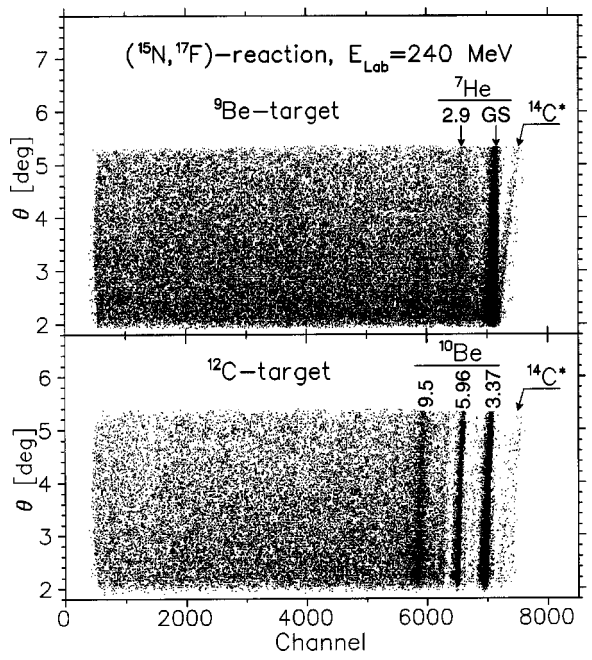

FIG. 1. Scatterplot of the scattering angle θ_{lab} of events vs the position in the focal plane for the (^{15}N,^{17}F) reaction on ^{9}Be (upper panel) and on ^{12}C (lower panel). Kinematical lines observed for the (^{15}N,^{17}F) reaction on ^{9}Be, ^{12}C, and ^{16}O target nuclei show different slopes. Kinematical corrections were applied to obtain for the ^{7}He ground state a straight line parallel to the θ_{lab} axis, therefore, the lines on ^{12}C and ^{16}O are tilted. Numbers correspond to excitation energies in MeV, the indicated ^{14}C* line (from the ^{16}O contamination) is the excited state at 7.01 MeV.

obtained results. This lower resolution is due to the larger energy-loss difference between ^{15}N and ^{17}F in the thicker target.

On the ^{12}C target [Fig. 2(c)] three 2^+ states in ^{10}Be at 3.37 MeV, 5.96 MeV, and 7.54 MeV (the latter as a part of a doublet with a 3^- state at 7.37 MeV) are observed. They are populated by the reaction mechanism of picking two protons from the $1p3/2$ and $1p1/2$ shells with different couplings. The population of the 3^- state at $E_x = 7.37$ MeV and a 4^- state at $E_x = 9.27$ MeV requires the excitation of a neutron to the $1d5/2$ shell in a higher-order process. Furthermore, a strong state at 9.55 MeV and two weak states at 10.5 MeV and 11.8 MeV are observed.

Three high-lying states of ^{10}Be are found at 13.6(1) MeV, 15.3(2) MeV, and 16.9(2) MeV with widths of 0.20(5) MeV, 0.8(2) MeV, and 1.4(3) MeV, respectively. Freer *et al.* [21] also observed recently ^{10}Be states at similar positions: 13.2(4) MeV, 14.8(4) MeV, and structures at 16.1(5)–17.2(5) MeV, which correspond probably to the broad resonance observed in our data at 16.9(2) MeV.

The spectrum of the two proton pickup on the ^{12}C target [Fig. 2(c)] shows contributions from ^{13}C (labeled ^{11}Be and vertically hatched) and ^{16}O (labeled ^{14}C and diagonally hatched). The background with the very broad shape results from three-body processes as discussed in Sec. III.

The nucleus ^{17}F has one particle stable excited state, a

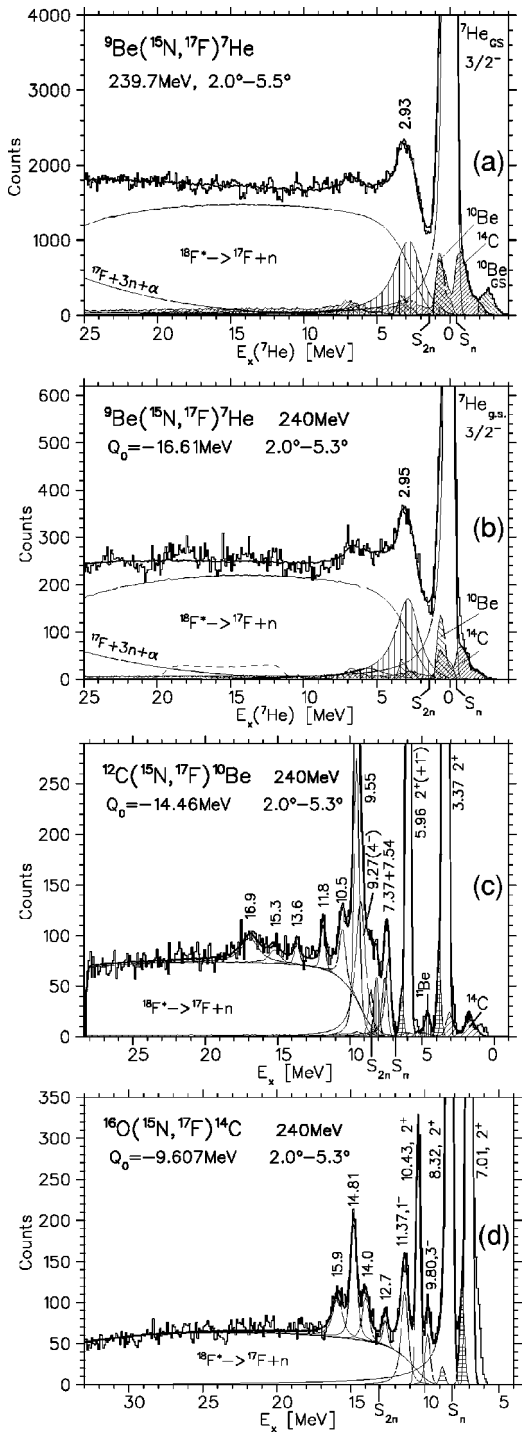

FIG. 2. Energy spectra of the (^{15}N,^{17}F) reaction are shown on ^{9}Be in panel (a) and, with better resolution, in panel (b); furthermore on ^{12}C in panel (c), and on ^{16}O in panel (d). The peak of the ^{7}He excited state is observed at about 2.95 MeV; a fit using a Breit-Wigner resonance (vertically hatched area) and the interpretation of the background in terms of three-body processes (^{18}F* $\rightarrow ^{17}$F$+n$) and the phase-space distribution of ^{17}F$+3n+\alpha$ is shown. Contributions from target contaminations ^{12}C and ^{16}O are indicated by the labels ^{10}Be (45° downward hatched area) and ^{14}C (45° upward hatched area), respectively. The horizontally hatched area corresponds to the excitation of ^{17}F at 0.495 MeV. In panel (c) the ground state of ^{10}Be is just out of range of the focal plane.

$1/2^{+}$ state at $E_x = 0.495$ MeV. With ^{17}F as the outgoing particle it is possible, that every state of the recoil nucleus appears twice in the spectrum: in combination with the ground state of ^{17}F and with its first excited state. We could analyze the contributions from the $1/2^{+}$ state in ^{17}F in the ^{12}C(^{15}N,^{17}F)^{10}Be reaction due to the good separation of the two strong ^{10}Be states at 3.37 MeV and 5.96 MeV (the latter line includes also a 1^{-} state, which is separated by only 1.7 keV from the 2^{+} state). The two 2^{+} states can be very well fitted by Gaussians using the energy resolution of 300 keV. Contributions from the ^{17}F$(1/2^{+})$ state at the known distance of 0.495 MeV are hardly seen, they are indicated in Fig. 2 (c) by the horizontally hatched areas on the left side of the strong peaks. The deduced cross sections are a factor of 40–50 smaller than for the ^{17}F$(5/2^{+})$ ground state. This demonstrates the strong dynamical suppression of the population of the *s* state as compared to a *d* state in a heavy-ion transfer reaction in this energy regime. We expect similar population ratios also in combination with other states of the recoil nucleus.

The spectrum of the ^{16}O(^{15}N,^{17}F)^{14}C reaction [see Fig. 2(d)] shows similar features as compared to the reaction on ^{12}C concerning the population of 2^{+} states and the one-neutron excitation to the $1d5/2$ shell, the 3^{-}, 1^{-} states. The highest-lying excited state of ^{14}C is observed at 15.9 MeV. Please note the very smooth shape of the three-body background in the spectra measured on ^{12}C and ^{16}O.

The spectra measured on ^{9}Be [Fig. 2(a), (b)] show a very strong line for the ground state of ^{7}He; the counting rate in the peak is 22 000 and 5000 counts per channel (100 keV/channel), respectively. *Low-lying* excited states of ^{7}He can involve only *neutron excitations* and can be populated in the two-proton pick-up reaction (^{15}N,^{17}F) only by a second order process. For this reason we expect a rather small cross section. We observe a clear peak above the background at 2.95 MeV excitation energy. However, the identification of this peak as an excited state of ^{7}He and the precise determination of the resonance energy and width needs a careful analysis of all background contributions (see Sec. III).

The 5.96 MeV state of ^{10}Be populated in the ^{12}C(^{15}N, ^{17}F)^{10}Be reaction on the carbon contamination of the ^{9}Be target is located just at the position of the excited state of ^{7}He. A direct normalization of the ^{10}Be background spectrum measured on the ^{12}C target, to a ^{10}Be contamination line in the ^{7}He spectrum [Fig. 2(b)] is not possible, especially since the well-separated line of the first excited state of ^{10}Be is hidden by the strong ^{7}He ground state. However, we can use the reaction channel ^{12}C(^{15}N, ^{14}O)^{13}B, where two strong excited states of ^{13}B at 6.43 MeV and 10.22 MeV [22] were observed, to determine the absolute thickness of the carbon content in the ^{9}Be target. The normalization of the ^{16}O content in the ^{9}Be target has been performed in a similar way using the ^{14}O exit channel. The ^{14}O spectrum is measured simultaneously with the ^{17}F spectrum in the focal plane, because both reactions have nearly the same magnetic rigidity, therefore the conditions of the measurements are identical.

The fit shown in Fig. 2(b) includes the normalized spectra

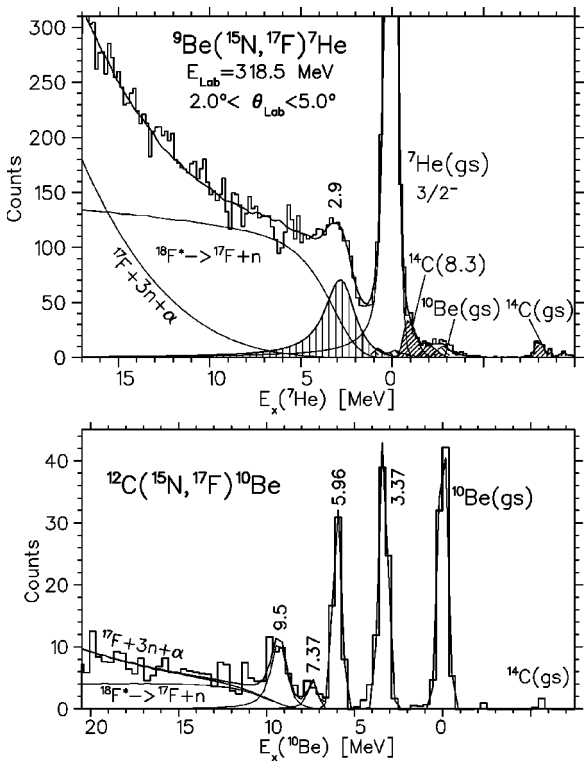

FIG. 3. Spectra of the ^{9}Be(^{15}N,^{17}F)^{7}He (upper panel) and ^{12}C(^{15}N,^{17}F)^{10}Be (lower panel) reactions at $E_{lab}=318.5$ MeV. The excited state of ^{7}He is observed in this fit at 2.9 MeV. The fit of the spectrum is discussed in Sec. IV and details of the background calculation in Sec. III.

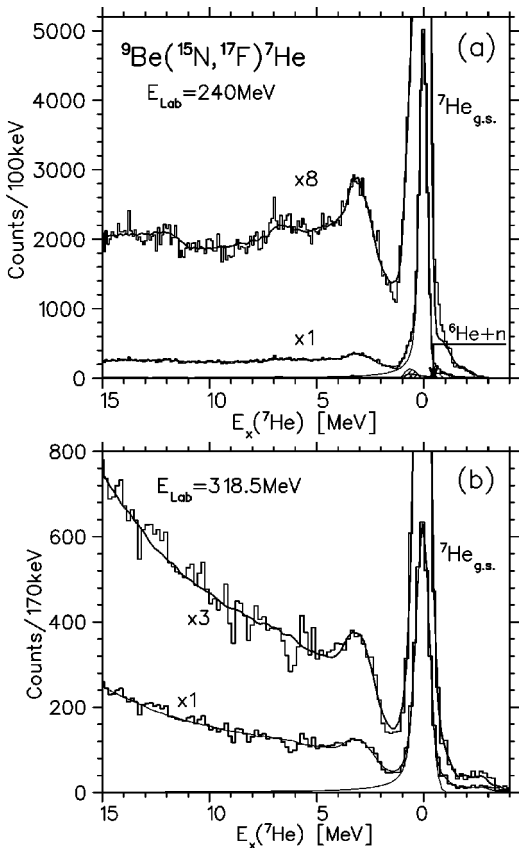

FIG. 4. Comparison of the spectra of the ^{9}Be(^{15}N,^{17}F)^{7}He reaction (a) at $E_{lab}=240$ MeV and (b) at 318.5 MeV. A bump is observed in both cases at the same place (~2.9 MeV). The thick solid lines represent the result of the fits.

on the contaminations ^{12}C and ^{16}O; they were measured for the full angular range with exactly the same field settings as for ^{9}Be. These normalized contributions are by far too small to explain the peak at 2.95 MeV excitation energy.

The ^{9}Be(^{15}N,^{17}F)^{7}He reaction has also been measured at higher incident energy, $E_{lab}=318.5$ MeV, with an angular opening $2.0°<\theta_{lab}<5.0°$ on a target of 450 μg/cm^2 thickness. The energy resolution is 600 keV in this case (Fig. 3, upper panel). The spectrum has been calibrated by the (^{15}N,^{17}F) reaction on ^{12}C (Fig. 3, lower panel). The ^{7}He excited state is again observed at about 2.9 MeV excitation energy, but the position is not as precisely determined as at 240 MeV due to the worse resolution. It is separated from the ground state again by the same characteristic deep minimum as at 240 MeV. The background at higher excitation energies rises faster due to the enhanced contributions of the ^{17}F $+3n+\alpha$ phase-space distribution at the higher incident energy.

In Fig. 4 the ^{17}F spectra measured at 240 MeV and 318.5 MeV are plotted for the same range of excitation energies. This direct comparison shows, which structures move or do not move with the incident energy. In the latter case the structures correspond to the excitation strength of the recoil nucleus ^{7}He, independent on the later decay of the unbound system. This is the characteristic signature for the binary character of a direct reaction. The peak at 2.95 MeV excitation energy stays at the same place (within the experimental errors) at both incident energies. This proves that we really observe an excited state of ^{7}He. Structures in the spectrum originating from a sequential decay mechanism would move, as is discussed in the next section.

Please note: An excited state above the neutron threshold $S(n)$ has a resonance energy E_R, which is related to the excitation energy E_x of the state by $E_R=E_x-S(n)$. The excitation energy scale (E_x) can be converted into a decay energy scale by $E_{decay}=E_x-S(n)$.

III. ANALYSIS OF THE THREE-BODY BACKGROUND

A. Mechanisms

The main part of the continuous background observed in the spectra is due to three-body processes with the three particles ^{17}F+n+^{6}He in the exit channel, where only ^{17}F is detected. In this case a continuous energy distribution is obtained due to incomplete reconstruction of the kinematics. The ^{6}He recoil nucleus may be emitted in its ground state or in excited states (in the latter case it will decay into ^{4}He $+2n$). For the extraction of the resonance parameters of ^{7}He excited states we are especially interested in the shape of the three-body background in the region from the ground state of ^{7}He to about 10 MeV excitation energy.

Two mechanisms are important in our considerations (see Fig. 5):

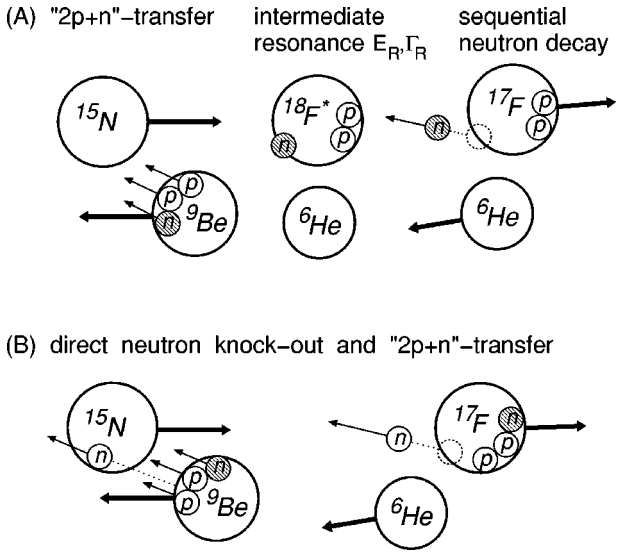

FIG. 5. Three-body processes shown in the c.m. system, which are important for background contributions to the ^{17}F spectrum in the region near the neutron threshold (^{6}He$+n$): (a) A neutron is transferred in addition to the two proton pickup to the projectile into an intermediate resonance, which emits in a sequential decay process the neutron again. (b) During a $(2p+n)$ transfer to the projectile a neutron is knocked out from the projectile by the target into *backward* direction through the neutron-target interaction.

(a) The sequential neutron decay of an intermediate outgoing particle formed in a resonance state via a transfer reaction into the detected particle, and

(b) The direct neutron knockout from the projectile by the target into *backward direction*, accompanied by the transfer of nucleons to form the detected outgoing particle (^{17}F).

In process (a) the transferred neutron (indicated in Fig. 5 by the hatched filling) forms a resonance of the ejectile (an *intermediate state* with a lifetime given by the width of the resonance) and is emitted in a sequential decay, whereas in process (b) it stays in the ejectile ^{17}F after the transfer; another neutron of the projectile has been knocked out before by the target.

Both processes contribute in the ^{17}F spectrum on the high-energy side near the threshold of the considered three-body channel, i.e., the ^{17}F$+n+^6$He threshold in the present case, when the neutron is emitted into backward direction. It is the characteristic difference between the two mechanisms, that in the first case the decay strength distribution is always the same, since it is defined by the resonance parameters E_R, Γ_R, of the decaying ^{18}F* resonance independent of the beam energy, whereas in the second case the mean energy and width of the energy distribution of the knocked-out neutron in the center-of-mass (c.m.) system will increase with increasing beam energy due to the increasing momentum transfer in the knockout process.

B. Sequential decay distributions

A pure three-body phase-space distribution of ^{17}F$+n+^6$He is not expected, since the particles interact with each other. In process (a) this concerns in particular the interaction

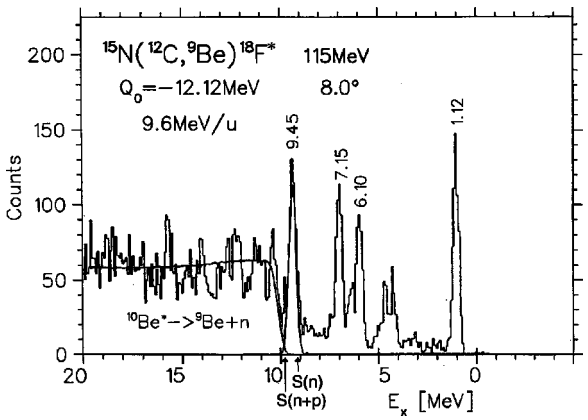

FIG. 6. Spectrum of the ^{15}N(^{12}C,^{9}Be)^{18}F reaction at $E_{lab}=115$ MeV measured by Rae *et al.* [26]. The neutron threshold $S(n)=9.15$ MeV and the neutron+proton threshold $S(n+p)=9.75$ MeV are indicated.

between the neutron and ^{17}F, where these two particles may be in a resonance state of ^{18}F. These resonances can be populated directly in the $(2p+n)$ transfer to the projectile. The ^{18}F$+^6$He channel contributes as an intermediate *binary channel* to the ^{17}F spectrum through the neutron decay of ^{18}F*. Hence, in this process the detected ^{17}F has been formed as a decay product of an intermediate ^{18}F* resonance. At the resonance the cross sections are enhanced in the ^{17}F$+n$ subsystem, the decay, however, can occur into all available open decay channels. The decay of ^{18}F* resonances into the following two-decay channels are important for our considerations:

(i) ^{18}F*$\rightarrow^{17}$F$+n$, $S(n)=9.15$ MeV,

(ii) ^{18}F*$\rightarrow^{16}$O$+p+n$, $S(n+p)=9.75$ MeV.

In this case the background observed in the ^{17}F spectra is produced in the decay branch (i) of the resonance, whereas strong decays into other branches like (ii) reduce those contributions. Therefore we do not expect all observed resonances above the neutron threshold of ^{18}F as decay distributions in the ^{17}F spectrum, when other decay channels are open.

As a result of the sequential decay, Fig. 5(a), characteristic shapes of the energy distributions are observed. For example, the decay of a narrow resonance ^{18}F*$\rightarrow^{17}$F$+n$ produces in the ^{17}F spectrum a broad energy distribution with a characteristic width depending on the decay energy E_{dec} in the ^{18}F* c.m. system and the velocity β of the ^{18}F* particle in the laboratory system (lab system) [23,24]. The same effect is known as Doppler broadening for γ emission in flight [25].

The population of ^{18}F states has been studied by Rae *et al.* [26] with the ^{15}N(^{12}C,^{9}Be)^{18}F* reaction at $E_{lab}=115$ MeV. The experimental spectrum (Fig. 6) shows only one strong line above the neutron threshold, the state at 9.45 MeV excitation energy; no other strong states of ^{18}F* are observed in this region. Excited states of ^{9}Be are not contributing, since ^{9}Be has no particle-stable excited states. The increased counting rate in the energy region above 10 MeV excitation energy (Fig. 6) is related to the open three-body channel. This region can be described by a sequential decay

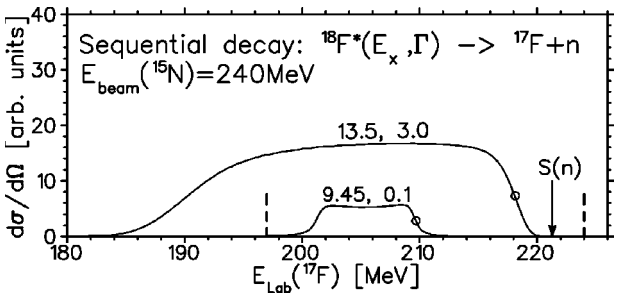

FIG. 7. Energy distributions in the lab system of ^{17}F ejectiles after the neutron decay in flight of excited ^{18}F* to the ground state of ^{17}F for the (^{15}N,^{18}F) reaction at 240 MeV. The decay strength distribution is characterized by the excitation energy E_x and width Γ of resonances in ^{18}F. The resulting energy distributions of ^{17}F are labeled by these values. The open circles indicate the maximum energy shifts for the given resonance energies $E_R=E_x-S(n)$. The two vertical dashed lines mark the energy range shown in Fig. 2.

distribution from the decay of ^{10}Be* resonances at around 9.5 MeV excitation energy into $^9\mathrm{Be}+n$. The population strength of these states in ^{10}Be is observed in our own measurement, see Fig. 2 (c).

The cross section for the ^{18}F(9.45 MeV) state populated in the $(2p+n)$ transfer depends on the spectroscopic factor S_1 describing the coupling strength of the transferred three nucleons to ^{15}N to form this resonance, and on the corresponding target spectroscopic factor S_2, from where they are taken. The factor S_1 remains the same for all targets, only S_2 scales the cross section with a target dependence. The shape of the energy distribution, which results from the decay of the ^{18}F(9.45 MeV) resonance, is shown in Fig. 7. A structure of this shape should appear in all the four spectra of Fig. 2, if the cross section is sufficiently large, but there is no clear indication in any of the spectra. Only in Fig. 2(b) there is some agreement of the position and width of the calculated decay distribution [dashed line in Fig. 2(b)] with a weak, corresponding structure in the experimental spectrum.

In the calculation of the shape of a sequential decay distribution (SDD) a forward-peaked angular distribution is used for the intermediate binary channel as well as a parametrization of the angular correlation function of the neutron decay. An asymmetry in the neutron angular distribution is taken into account by the parametrization $1+a\cos^2(\theta_n)$. The distributions shown in Fig. 7 were calculated by numerical integration over polar and azimuthal emission angles of the light particle, taking into account the angular shifts of the ejectile introduced by the light particle emission, and over the relevant range of decay energies, which is defined by the decay strength distribution in ^{18}F. This strength distribution is parametrized either by a Breit-Wigner line shape at the corresponding excitation energy for a known single resonance, or by a Gaussian for a more general parametrization of a broad strength distribution. An SDD shows relatively sharp edges for a narrow width ($\Gamma_R=0.1-0.5$ MeV) of a decaying strength distribution. Some details of the formalism are given in Ref. [23], but the corresponding code has been extended considerably since then [27].

The main part of the three-body background in all the ^{17}F spectra of Fig. 2 rises within a few MeV starting from a place not far from the neutron threshold up to a level, which is then almost constant over the full range to the maximum detected excitation energy; this is, e.g., for the ^{16}O target at 33 MeV. Assuming a common mechanism for these very similar distributions on all the three targets, we described this background in a first attempt by the sequential decay distribution. For the source of this background the decay of one broad resonance in ^{18}F (in addition to the 9.45 MeV state) is sufficient. The following resonance parameters (E_{decay}, Γ) were found to fit the background in the spectra on ^{9}Be, ^{12}C, and ^{16}O:

$E_x(^{18}\mathrm{F})=13.5$ MeV ($E_{decay}=4.35$ MeV), $\Gamma=3.0$ MeV.

A true resonance, however, is not observed in Fig. 6 at this place. The decay distribution calculated with these parameters is shown in its full width in Fig. 7 vs the energy in the lab system of the detected ^{17}F. At the low-energy side the calculated energy distribution decreases again to zero (Fig. 7). The measurement has not been extended to this energy range, but it is also not expected in any case, that on this low-energy side the calculated shape would be observable in a measurement, since other processes will contribute more and more at higher-energy losses. [We want to note, that contributions from the sequential decay of excited ^{19}F resonances to the decay channel $^{17}\mathrm{F}+2n$ cannot explain the observed background distributions near the threshold region in a consistent way, since for the ^{16}O target the *observed* distribution rises already far beyond the two-neutron threshold, see Fig. 2(d).]

If the parametrized strength distribution in ^{18}F would represent a true resonance, then it should be possible by increasing the incident energy, to move the whole SDD to higher excitation energies, i.e., further away from the first excited state of ^{7}He.

In order to test this idea and to investigate in more details the origin of the background, we have measured the $^9\mathrm{Be}(^{15}\mathrm{N},^{17}\mathrm{F})^7\mathrm{He}$ reaction at 318.5 MeV (21.2 MeV/nucleon) incident energy. To show for a resonance at the given excitation energy E_x the expected dependence of the maximum energy shift (Fig. 7, open circle) on the beam energy, we calculate the *maximum* energy of ^{17}F ejectiles in forward direction in the lab system, $E_{max}(^{17}\mathrm{F},\mathrm{SDD})$, obtained in the neutron decay of ^{18}F* for discrete E_x values. This energy E_{max} is plotted in Fig. 8 with respect to the ^{17}F kinetic energy $E_{thresh}(^{17}\mathrm{F})$ of the $^9\mathrm{Be}(^{15}\mathrm{N},^{17}\mathrm{F})$ reaction at the neutron threshold. The formulas to calculate this energy difference are given in the Appendix. The result is plotted for ^{18}F decay energies $E_{decay}(^{18}\mathrm{F})=0,\ 1,\ 4.35,\ 10$ MeV corresponding to excitation energies $E_x(^{18}\mathrm{F})=9.15$ MeV, 10.15 MeV, 13.5 MeV, 19.15 MeV, respectively.

One can see in Fig. 8, that for $E_x=13.5$ MeV the energy difference $|E_{max}-E_{thresh}|$ increases from 3.3 MeV at 240 MeV incident energy to 6.1 MeV at 318.5 MeV, the dashed arrow indicates the expected shift. At the latter beam energy a clear separation between the high-energy side of the SDD and the first excited state of ^{7}He is expected. However, the measured spectrum does not show the full shift (Fig. 9). The SDD shown by the short-dashed line has been calculated

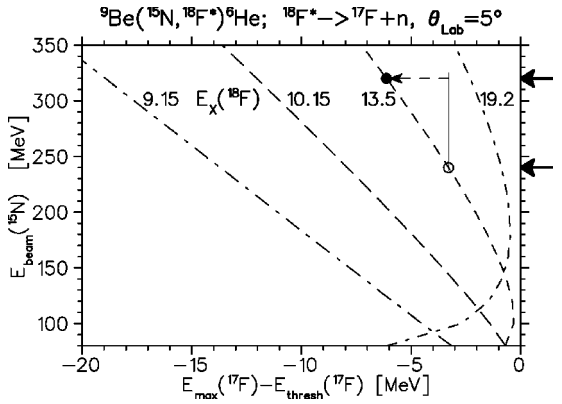

FIG. 8. Maximum energies E_{max} in the lab system of ^{17}F resulting from the neutron decay of highly excited ^{18}F ejectiles in the ^{9}Be(^{15}N,^{18}F*)^{6}He reaction as a function of the beam energy E_{beam} of the ^{15}N projectiles. The plotted quantity $E_{max}-E_{thresh}$ shows E_{max} with respect to the ^{17}F energies at the neutron threshold, E_{thresh}. The excitation energies $E_x(^{18}\mathrm{F})$ are given as parameters at the curves. The arrows on the right indicate the beam energies used in this work.

using the same resonance parameters of ^{18}F* as determined at 240 MeV ($E_x=13.5$ MeV, $E_{decay}=4.35$ MeV, $\Gamma=3.0$ MeV). The resulting sum of calculated contributions (short-dashed lines), including a Breit-Wigner resonance in the region of 3 MeV excitation energy, does not fit the experimental spectrum, a broad dip remains at about 5 MeV.

A better fit is obtained (full lines in Fig. 9), when the *parametrized decay strength is moved to higher-decay energies*: $E_x(^{18}\mathrm{F}^*)=16$ MeV ($E_{decay}=6.8$ MeV) and $\Gamma=4.0$ MeV. As a result, a difference $|E_{max}-E_{thresh}|=4.6$ MeV is obtained. This is 1.5 MeV less than expected at 318.5 MeV incident energy, but still 1.3 MeV larger than 3.3 MeV obtained at 240 MeV. This observation is in agreement with a recent systematic analysis [28] of many spectra of heavy-ion transfer reactions between 15 MeV/nucleon and 30 MeV/nucleon, which revealed a clear correlation between the needed decay energy in the fit of the three-body background and the incident *energy per nucleon*. The higher value of the

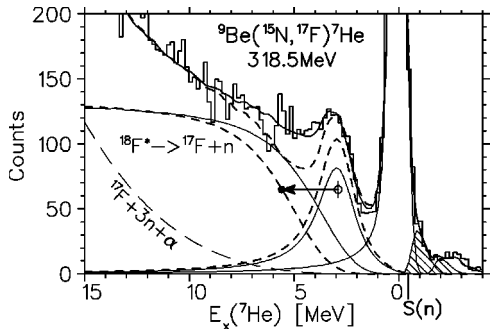

FIG. 9. Comparison of calculated three-body distributions for 318.5 MeV incident energy using the same resonance parameters for the decay strength distribution of ^{18}F as found at 240 MeV (short-dashed lines), or using larger values to obtain a good fit of the experimental spectrum (solid lines). In the former case a dip remains at about 5 MeV excitation energy.

mean decay energy (6.8 MeV) of ^{18}F* leads in the actual case to a reduced distance of only 4.6 MeV between $E_{max}(^{17}\mathrm{F}, \mathrm{SDD})$ and the neutron threshold.

C. The neutron knockout process

The needed increase of the mean decay energy with increasing beam energy indicates, that the main part of the observed three-body background does not result from the sequential decay of a broad resonance of ^{18}F [mechanism (a)], but more likely from the three-body mechanism (b), the knock out of a nucleon (neutron in this case) from the projectile by the target during the transfer of other particles [Fig. 5(b)]. The momentum transferred to the knocked-out nucleon increases with increasing energy/nucleon of the beam.

We are especially interested in the backward emission of the neutron, because only with this condition the detected ejectile can reach maximal momenta and energies near the three-body threshold. Since our spectra are measured at *very forward angles* in the region of maximum energy shifts in forward direction, the kinematical conditions are very similar for both mechanisms, (a) and (b), to describe the high-energy side of the ^{17}F energy distribution. They correspond almost to a back-to-back emission of ^{17}F and the neutron along the direction of ^{18}F* before the decay.

Therefore we approximate *at forward angles* the description of process (b) using distributions of the sequential neutron emission from a Gaussian strength distribution in the c.m. system of $^{17}\mathrm{F}+n$. The parameters of the Gaussian distributions are adjusted to obtain a good fit of the spectra. We consider this description of the background as a reasonable approximation and a good parametrization. At larger ^{17}F emission angles differences are expected for the energy distributions of the direct three-body process (b) and the sequential decay process (a).

IV. RESULTS FOR ^{7}He AND DISCUSSION

The spectra of the (^{15}N,^{17}F) reaction at 240 MeV incident energy have been measured with good energy resolution and high statistics; therefore we could analyze the resonance parameters of the first excited state of ^{7}He as well as the ones of the ground state.

A. The ground state

The resonance parameters of the ground state have been obtained by Stokes and Young [1] from the (t,^{3}He) reaction on ^{7}Li at $E_{lab}=22$ MeV using $\Delta E-E$ Si-detector telescopes. They found a width of $\Gamma=0.16(3)$ MeV for the ground state resonance at 0.44(3) MeV above the $^6\mathrm{He}+n$ threshold.

In the analysis of our measurements we included in the fit of the *observed line shape* the following contributions to describe the width: (i) the experimental resolution (300 keV), (ii) the energy-loss difference between ^{15}N and ^{17}F in the ^{9}Be target (350 keV), (iii) the resonance width Γ_R, which was searched for in the fit.

We use the following parametrization of a Breit-Wigner resonance with an energy-dependent width:

TABLE I. Results obtained in the analysis of the ^{9}Be(^{15}N,^{17}F)^{7}He reaction at 240 and 318.5 MeV, and comparison with other data. Spins and parities J^{π}, excitation energies E_x, resonance energies E_R, and widths Γ_R, differential cross sections $d\sigma/d\Omega$ (c.m.) in the c.m. system, and experimental resolutions δE are given.

J^{π}	$E_x(^{7}\mathrm{He})$ (MeV)	$E_R(^{6}\mathrm{He}+n)$ (MeV)	Γ_R (MeV)	$d\sigma/d\Omega$ (c.m.) (μb/sr)	δE (MeV)	References, remarks
$3/2^-$	0.00	0.44(3)	0.16(3)	50 – 300	0.16	Stokes and Young, 1967, 1969 [1]
						^{7}Li(t,^{3}He)^{7}He, 22 MeV, $\theta_{\mathrm{c.m.}}=10°-60°$
$(1/2^-)$	0.8(2)	1.2(2)	1.0(2)			Markenroth *et al.*, 2001 [19]
						^{8}He dissociation, 227 MeV/nucleon
	2.9(3)	3.3(3)	2.2(3)	~2000	1.5	Korsheninnikov *et al.*, 1999 [18]
						^{8}He(p,d)^{7}He, 50 MeV/nucleon, $\theta_{\mathrm{c.m.}}=6°-15°$
$(5/2^-)$				1600		Decay to $n+^{6}$He$(2^+)\rightarrow 3n+^{4}$He
				400		Decay to $n+^{6}$He (g.s.)
			This work			^{9}Be(^{15}N,^{17}F)^{7}He
$3/2^-$	0.00	0.44	0.14(2)	140(10)	0.3	240 MeV, $\theta_{\mathrm{c.m.}}=6.5°-17°$
$(1/2^-5/2^-)$	2.95(10)	3.39(10)	1.9(2)	22(5)	0.3	
	5.8(3)	6.2(3)	3 – 5	16(7)		
$(1/2^- - 5/2^-)$	2.90–3.00 (15)	3.34–3.44 (15)	1.8(3)		0.6	318.5 MeV, $\theta_{\mathrm{c.m.}}=6.4°-16°$
	5.8(3)	6.2(3)	3 – 5			

$$\sigma(E_{dec}) \sim \frac{\Gamma(E_{dec})}{[E_{dec}-E_R-\Delta(E_{dec})]^2+[\Gamma(E_{dec})/2]^2},$$

where the width

$$\Gamma(E_{dec}) = P_l(E_{dec})/P_l(E_R)\times\Gamma_R$$

is dependent on the decay energy E_{dec} and the decay angular momentum l through the penetrability $P_l(E_{dec})$. The latter quantity and the shift function $\Delta(E_{dec})$ are defined as usual [29]. A channel radius of 6 fm has been used in all cases.

A value $\Gamma_R=0.14(2)$ MeV (see Table I) is obtained with $l=1$ and $E_R=0.44(3)$ MeV for the ground state resonance (an absolute mass measurement of ^{7}He was not performed). This width is slightly smaller than the value of Stokes and Young, but both values overlap within the error bars. The same width also describes at 318.5 MeV the shape of the ground state line very well.

Figure 10 shows an expanded view of the ground state region of the spectrum at 240 MeV after subtraction of the background from ^{12}C and ^{16}O. The data (histogram, with error bars on the steps indicating the statistical error) are compared with the fit results using the best fit value for the width $\Gamma_R=0.14$ MeV (filled dots connected by solid lines) and values 20 keV larger (open triangles connected by dash-dotted lines) or smaller (open circles connected by dashed lines), respectively. The fits were performed in the range of excitation energies from -3.0 MeV to 9.0 MeV to include the effect of the extended tail of the Breit-Wigner resonance on the quality of the overall fit. The least-mean-square values per data point obtained in the fit are 1.87, 2.24, and 2.32 for $\Gamma_R=0.14$ MeV, 0.16 MeV, and 0.12 MeV, respectively.

To show more clearly the deviations of the three fits in Fig. 10 from the data histogram in the peak region, we use besides the different line codes also different plot symbols: filled dots for $\Gamma_R=140$ keV, open triangles for 160 keV, and open circles for 120 keV. The tail region is better seen with a scale factor of five: the solid line for the best fit ($\Gamma_R=140$ keV), and the two other line codes to see the quality of these fits. At the low-decay energy side the three curves show only very small differences due to the close vicinity of the threshold and the influence of the centrifugal barrier for the $l=1$ decay. At this side some counting rate still remains from the

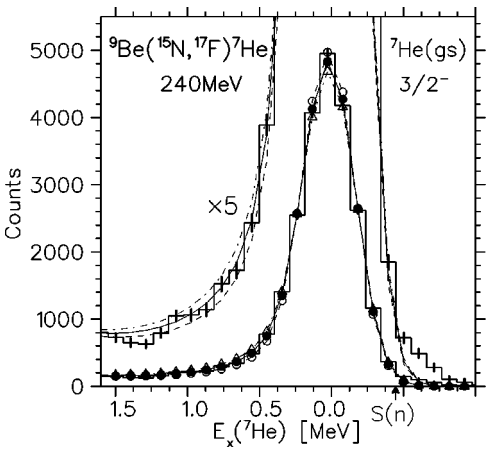

FIG. 10. Width of the ^{7}He ground state resonance: fits of the data (histogram) are shown for widths of 140 keV (best fit, filled dots connected by solid lines), 160 keV (open triangles and dash-dotted lines), and 120 keV (open circles and dashed lines), respectively.

oxygen contamination, because the shape of the spectrum measured on the V_2O_5 target is somewhat smoother than needed for a complete subtraction. However, using a spectrum on ^{16}O of better resolution would not reduce the difference between the Γ_R value from Stokes and Young and ours, on the contrary, our value would decrease even slightly more. The shape of the observed line is well described in the present fit by the width of 0.14 MeV, as Fig. 10 shows, and the two curves calculated with $\Gamma_R = 0.14 \pm 0.02$ MeV correspond to an error band.

B. Excited states

The excitation energy region in the ^{17}F spectra above the ^{7}He ground state resonance was analyzed using Breit-Wigner resonances, three-body distributions as discussed in Sec. III, five-body phase-space distribution for $^{17}\mathrm{F}+3n+\alpha$, and normalized background spectra for the target contaminations of ^{12}C and ^{16}O.

The excited state of ^{7}He at about 2.95 MeV is observed in our data at both incident energies of 240 and 318.5 MeV at a place, where the background is just rising. This might have a considerable effect on the determination of the position and width of the resonance in the analysis of the spectrum. There might be also further excitation strength of ^{7}He at excitation energies above the first excited state in the form of broader resonances, and indeed, there are indications of a small broad bump at 5.8 MeV excitation energy in the spectrum even after subtraction of the background spectra of ^{12}C and ^{16}O [see Fig. 2(b) and Fig. 11, upper panel]. The spectra on the ^{9}Be, ^{12}C, ^{16}O targets were measured at 240 MeV incident energy with good statistics, and especially on ^{12}C and ^{16}O the *shape* of the three-body background is very well defined (Fig. 2) and can be described using the same parameters (see Sec. III). Using these parameters also for ^{9}Be, a good fit of the spectrum is achieved as shown in Fig. 2(b), when two resonances of ^{7}He are introduced, one at 2.95(10) MeV and a second one in the region of 5.8 MeV excitation energy.

To be consistent, a ^{7}He resonance at 5.8 MeV excitation energy has been introduced also in the spectrum at 318.5 MeV incident energy. The three-body decay distribution is calculated in this case with slightly modified parameters, $E_x = 14$ MeV ($E_{decay} = 4.85$ MeV), $\Gamma = 6$ MeV. Also the position of the first excited state changes a little by this modification: $E_x(^7\mathrm{He}) = 3.00(15)$ MeV. The corresponding fit is shown in the lower panel of Fig. 11, the background from ^{12}C and ^{16}O has been subtracted in the plot. The width of the 5.8 MeV resonance is large at both incident energies, values of Γ_R between 3 and 5 MeV could be used in the fit.

In the three spectra of the $^9\mathrm{Be}(^{15}\mathrm{N},^{17}\mathrm{F})^7\mathrm{He}$ measurements [Figs. 2(a), 2(b), and 3] the first excited state of ^{7}He is observed at the mean value of 2.95(10) MeV excitation energy (Table I) with a width of 1.9(2) MeV using $l = 1$ as the decay angular momentum. This result is in good agreement with the findings of Korsheninnikov *et al.* [18] (see Table I), who used the $p(^8\mathrm{He},d)^7\mathrm{He}$ reaction. These authors also measured the outgoing deuteron in coincidence with ^{6}He and ^{4}He as decay products from ^{7}He. Comparing the spectra of Figs. 2(b), 2(c), and 2(d) of Ref. [18], about 80% of the cross

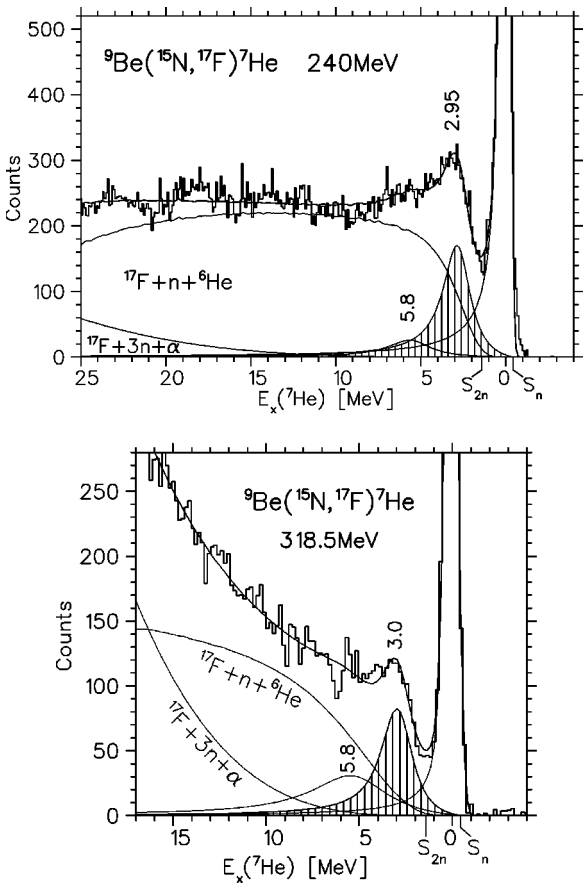

FIG. 11. Fit of the spectra of the $^9\mathrm{Be}(^{15}\mathrm{N},^{17}\mathrm{F})^7\mathrm{He}$ reactions at 240 MeV (upper panel) and 318.5 MeV (lower panel) including a Breit-Wigner resonance at 2.95 MeV and 3.0 MeV, respectively, and an additional ^{7}He resonance at 5.8 MeV excitation energy.

section ($\sim$2 mb/sr) at the observed peak decays into ^{4}He [Fig. 2(d)], whereas the remaining part is detected in coincidence with ^{6}He [Fig. 2(c)]. The authors concluded, that the decay into ^{4}He occurs via the $^6\mathrm{He}(2^+)$ state at 1.8 MeV, which is particle unstable against $2n$ emission, and deduced a spin-parity assignment of $5/2^-$ for this state. This implies a configuration of a $1p1/2$-neutron coupled to a core-excited 2^+ state of ^{6}He. A possible $3/2^-$ coupling was excluded, because the calculations of Wurzer and Hofmann [14] did not show any $3/2^-$ resonance (except the ground state of ^{7}He) up to 20 MeV excitation energy.

The structure of the 5.8 MeV resonance can only be estimated from theoretical calculations, which predict in this excitation energy region states with spin parities $5/2^+$ [13], $5/2^-$ [13,14], and $3/2^-$ [12,16].

Concerning the part of the peak at 2.9 MeV, which is observed in Ref. [18] in coincidence with ^{6}He, the authors suggested that this cross section might be attributed to an additional resonance in this region. Such a resonance should have the structure of a ^{6}He core in its ground state and a neutron in a single-particle orbit, e.g., $1/2^-$ [14] or $5/2^+$, and there might be indeed one of these states at this place. We note that all theoretical calculations obtain a $1/2^-$ resonance as the lowest-lying excited state of ^{7}He. The broad higher-

lying resonance at 5.8 MeV, which we observe in our measurements, may still contribute considerably in the region of the 2.9 MeV resonance, but it cannot explain the strength observed in Ref. [18] in coincidence with ^{6}He, since the latter shows only a width of 2.2 MeV.

V. SUMMARY

States of ^{7}He have been studied using the two-proton pick-up reaction ^{9}Be(^{15}N,^{17}F)^{7}He at 240 MeV and 318.5 MeV. The strong population of the ground state resonance and the good resolution at 240 MeV allowed us to analyze the line shape of the ground state, and a width of $\Gamma_R = 0.14(2)$ MeV was obtained. An excited state could be clearly identified at 2.95(10) MeV excitation energy [corresponding to a resonance energy $E_R = 3.39(10)$ MeV] with a width $\Gamma_R = 1.9(2)$ MeV. In the region between these states there was no indication of a resonance, i.e., at about 0.8 MeV excitation energy as in Ref. [19]. The measured shape of the ground state resonance is described very precisely from the top (5000 counts/channel, Fig. 10) down to the tail at about 100 counts/channel (Figs. 10 and 11) by the analyzed width, a further resonance would not fit the data.

We made strong efforts to understand the origin of the continuous background to be able to describe it in a systematic way and separate it from the true excitation strength of ^{7}He. For this reason we measured the (^{15}N,^{17}F) reaction at two incident energies and found, that in the present case the sequential decay mechanism cannot account correctly for the observed energy dependence of the main part of the background in the ^{17}F spectra. A better description is obtained with the mechanism of a neutron knockout, which is consistent for the energy dependence (240 and 318.5 MeV) and for different target nuclei (^{9}Be, ^{12}C, ^{16}O). Using this systematics of the background shape, we found evidence for a further ^{7}He resonance at 5.8 MeV excitation energy with a large width between 3 and 5 MeV.

ACKNOWLEDGMENTS

This work was supported by the BMBF Project No. 06 OB 47204, by the NATO Linkage Grant No. 960375, and by U.S. Department of Energy Grant No. DE-FG02-88ER40387.

APPENDIX

We want to calculate, how closely a three-body distribution of a given decay energy approaches the three-body threshold in a spectrum of the corresponding two-body reaction. This is of interest, because the three-body distribution forms a continuous background for the excited states of the two-body channel. The three-body distribution is very disturbing when it approaches the three-body threshold. The highest lab energy of the three-body distribution is called in the following E_{max}, and we calculate this quantity for a SDD, for the example of the present reaction.

The maximum energy of an SDD is obtained for a given excitation energy E_x of ^{18}F in the following way in *relativistic kinematics* (the equations are derived using basic kinematical relations from Ref. [30]):

$$E_{max}^{SDD}(^{17}F) = \gamma(^{18}\mathrm{F}^*)\ E_{\mathrm{c.m.},^{18}\mathrm{F}^*}(^{17}\mathrm{F}) \times [1+\beta(^{18}\mathrm{F}^*)\ \beta_{\mathrm{c.m.},^{18}\mathrm{F}^*}(^{17}\mathrm{F})] \quad \text{(A1)}$$

with $\beta(^{18}\mathrm{F}^*)$ and $\gamma(^{18}\mathrm{F}^*)$ the velocity and γ factor of the outgoing ^{18}F* excited with the excitation energy $E_x = E_{decay} + S_n$ (S_n neutron separation energy of ^{18}F). The energies are total energies including the rest mass (except E_x, E_{decay}). The maximum energy of Eq. (A1) is obtained for the condition, that the momenta of ^{18}F* and the neutron are antiparallel, the neutron is emitted in this case at 180° with respect to the direction of the ^{18}F*. The values of β and γ are obtained from a relativistic two-body kinematical program for the actual reaction, ^{9}Be(^{15}N,^{18}F*)^{6}He in our case.

In Eq. (A1) the energy of ^{17}F in the rest frame of the decaying ^{18}F* is given by

$$E_{\mathrm{c.m.},^{18}\mathrm{F}^*}(^{17}\mathrm{F}) = \frac{1}{2M(^{18}\mathrm{F}^*)}[M(^{18}\mathrm{F}^*)^2 + M(^{17}\mathrm{F})^2 - M(n)^2] \quad \text{(A2)}$$

with $M(^AZ)$ the rest mass of isotope ^AZ. The quantity $\beta_{\mathrm{c.m.},^{18}F^*}(^{17}\mathrm{F})$ in Eq. (A1) is the ^{17}F velocity in the rest frame of ^{18}F*, it is obtained from $E_{\mathrm{c.m.},^{18}\mathrm{F}^*}(^{17}\mathrm{F})$, Eq. (A2):

$$\gamma_{\mathrm{c.m.},^{18}\mathrm{F}^*}(^{17}\mathrm{F}) = \frac{E_{\mathrm{c.m.},^{18}\mathrm{F}^*}(^{17}\mathrm{F})}{M(^{17}\mathrm{F})}, \quad \text{(A3)}$$

and using the general definition of γ: $\gamma = [1-\beta^2]^{-1/2}$. The quantities in Eq. (A1) with the index (c.m.,^{18}F*) are independent on the incident energy, whereas $\gamma(^{18}\mathrm{F}^*)$ and $\beta(^{18}\mathrm{F}^*)$ are dependent. These dependencies determine the exact behavior at the high-energy side of an SDD. The values of $E_{max}^{SDD}(^{17}\mathrm{F})$ and the maximum kinetic energy

$$T_{max}(^{17}\mathrm{F}) = E_{max}^{SDD}(^{17}\mathrm{F}) - M(^{17}\mathrm{F})$$

can be calculated in this way from Eqs. (A1)–(A3).

In the approximation of *nonrelativistic kinematics* the momentum of the outgoing ^{17}F results from the vector sum of the momenta of ^{18}F* in the lab system and the recoil momentum of the neutron in the ^{18}F* c.m. system [with $\mathbf{p}_{\mathrm{c.m.},^{18}\mathrm{F}^*}(n) = -\mathbf{p}_{\mathrm{c.m.},^{18}\mathrm{F}^*}(^{17}\mathrm{F})$],

$$\mathbf{p}_{lab}(^{17}\mathrm{F}) = \mathbf{p}_{lab}(^{18}\mathrm{F}^*) + \mathbf{p}_{\mathrm{c.m.},^{18}\mathrm{F}^*}(^{17}\mathrm{F}).$$

The expression for the ^{17}F energy in the lab system therefore contains the product of both velocities. This product $\beta(^{18}\mathrm{F}^*)\beta_{\mathrm{c.m.},^{18}\mathrm{F}^*}(^{17}\mathrm{F})$ introduces the peculiar kinematical square-root dependence for the maximum energy shift on the decay energy and on the lab energy of ^{18}F*. Due to this dependence, an increase of the incident energy leads to a larger distance between the maximum energy of an SDD and the energy of an ^{17}F ejectile produced directly in a binary reaction, $A(^{15}\mathrm{N},^{17}\mathrm{F})B_{\mathrm{g.s.}}$, on a target A for the ground state of B as a reference energy.

[1] R.H. Stokes and P.G. Young Phys. Rev. Lett. **18**, 611 (1967); Phys. Rev. **178**, 2024 (1969).
[2] R.B. Weisenmiller, N.A. Jelley, D. Ashery, K.H. Wilcox, G.J. Wozniak, M.S. Zisman, and J. Cerny, Nucl. Phys. **A280**, 217 (1977).
[3] D.V. Aleksandrov, Y.A. Glukov, B.G. Novatskii, E.Yu. Nikolskii, A.A. Ogloblin, and D.N. Stepanov, Izv. Akad. Nauk (USSR) **49**, 2115 (1985).
[4] J.P. Perroud, A. Perrenoud, J.C. Alder, B. Gabioud, C. Joseph, J.F. Loude, N. Morel, M.T. Tran, E. Winkelmann, H. von Fellenberg, G. Strassner, P. Truöl, W. Dahme, H. Panke, and D. Renker, Nucl. Phys. **A453**, 542 (1986).
[5] H.G. Bohlen, in *Proceedings of the International Symposium on Structure and Reactions of Unstable Nuclei*, Niigata, Japan, 1991, edited by K. Ikeda, Y. Suzuki (World Scientific, Singapore, 1991), p. 83.
[6] H.G. Bohlen, B. Gebauer, Th. Kirchner, M. von Lucke-Petsch, W. von Oertzen, A.N. Ostrowski, Ch. Seyfert, Th. Stolla, M. Wilpert, Th. Wilpert, S.M. Grimes, T.N. Massey, R. Kalpakchieva, Y.E. Penionzhkevich, D.V. Alexandrov, I. Mukha, A.A. Ogloblin, and C. Detraz, Nucl. Phys. **A583**, 775 (1995).
[7] F. Ajzenberg-Selove, Nucl. Phys. **A490**, 51 (1988).
[8] K.K. Seth, Phys. Rev. Lett. **58**, 1930 (1987).
[9] H.G. Bohlen, in *Proceedings of the International School-Seminar on Heavy-Ion Physics, Dubna, Russia, 1993*, edited by Yu.Ts. Oganessian, Yu.E. Penionzhkevich, and R. Kalpakchieva (JINR, Dubna, 1993), p. 17.
[10] W. von Oertzen, H.G. Bohlen, B. Gebauer, M. von Lucke-Petsch, A.N. Ostrowski, Ch. Seyfert, Th. Stolla, M. Wilpert, Th. Wilpert, D.V. Alexandrov, A.A. Korsheninnikov, I. Mukha, A.A. Ogloblin, R. Kalpakchieva, Y.E. Penionzhkevich, S. Piskor, S.M. Grimes, and T.N. Massey, Nucl. Phys. **A588**, 129c (1995).
[11] A. Csótó and G.M. Hale, Phys. Rev. C **55**, 536 (1997).
[12] A.A. Wolters, A.G.M. van Hees, and P.W.M. Glaudemans, Phys. Rev. C **42**, 2062 (1990).
[13] N.A.F.M. Poppelier, A.A. Wolters, and P.W.M. Glaudemans, Z. Phys. A **346**, 11 (1993).
[14] J. Wurzer and H.M. Hofmann, Phys. Rev. C **55**, 688 (1997).
[15] B.S. Pudliner, V.R. Pandharipande, J. Carlson, S.C. Pieper, and R.B. Wiringa, Phys. Rev. C **56**, 1720 (1997).
[16] P. Navrátil and B.R. Barrett, Phys. Rev. C **57**, 3119 (1998).
[17] H.G. Bohlen, W. von Oertzen, R. Kalpakchieva, A. Blažević, B. Gebauer, S.M. Grimes, A. Lépine-Szily, T.N. Massey, W. Mittig, A.N. Ostrowski, J.M. Oliveira, P. Roussel-Chomaz, S. Thummerer, and M. Wilpert, *Proceedings of SNEC98 Conference*, Padua, 1998, edited by S. Lunardi, R.A. Ricci, and W. von Oertzen [Nuovo Cimento Soc. Ital. Fis., A **111A**, 841 (1998)].
[18] A.A. Korsheninnikov, M.S. Golovkov, A. Ozawa, E.A. Kuzmin, E.Yu. Nikolskii, K. Yoshida, B.G. Novatskii, A.A. Ogloblin, I. Tanihata, Z. Fulop, K. Kusaka, K. Morimoto, H. Otsu, H. Petrascu, and F. Tokamai, Phys. Rev. Lett. **82**, 3581 (1999).
[19] K. Markenroth, M. Meister, B. Eberlein, D. Aleksandrov, T. Aumann, L. Axelsson, T. Baumann, M.J.G. Borge, L.V. Chulkov, W. Dostal, Th.W. Elze, H. Emling, H. Geissel, A. Grünschloß, M. Hellström, J. Holeczek, B. Jonson, J.V. Kratz, R. Kulessa, A. Leistenschneider, I. Mukha, G. Münzenberg, F. Nickel, T. Nilsson, G. Nyman, M. Pfützner, V. Pribora, A. Richter, K. Riisager, C. Scheidenberger, G. Schrieder, H. Simon, J. Stroht, O. Tengblad, and M.V. Zhukov, Nucl. Phys. **A679**, 462 (2001).
[20] M. Thoennessen, S. Yokoyama, A. Azhari, T. Baumann, J.A. Brown, A. Galonsky, P.G. Hansen, J.H. Kelly, R.A. Kryger, E. Ramakrishnan, and P. Thirolf, Phys. Rev. C **59**, 111 (1999).
[21] M. Freer, J.C. Angélique, L. Axelsson, B. Benoit, U. Bergmann, W.N. Catford, S.P.G. Chappell, N.M. Clarke, N. Curtis, A. D'Arrigo, E. de Goóes Brennard, O. Dorvaux, B.R. Fulton, G. Giardina, C. Gregori, S. Grévy, F. Hanappe, G. Kelly, M. Labiche, C. Le Brun, E. Leenhardt, M. Lewitowicz, K. Markenroth, F.M. Marqués, J.T. Murgatroyd, T. Nilsson, A. Ninane, N.A. Orr, I. Piqueras, M.G. Saint Laurent, S.M. Singer, O. Sorlin, L. Stuttgé, and D.L. Watson, Phys. Rev. C **63**, 034301 (2001).
[22] R. Kalpakchieva, H.G. Bohlen, W. von Oertzen, B. Gebauer, M. von Lucke-Petsch, T.N. Massey, A.N. Ostrowski, Th. Stolla, M. Wilpert, and Th. Wilpert, Eur. Phys. J. A **7**, 451 (2000).
[23] H.G. Bohlen, H. Ossenbrink, H. Lettau, and W. von Oertzen, Z. Phys. A **320**, 237 (1985).
[24] E. Adamides, H.G. Bohlen, W. von Oertzen, M. Buenerd, J. Chauvin, D. Lebrun, J.Y. Hostachy, Ph. Martin, G. Perrin, and P. de Saintignon, Nucl. Phys. **A475**, 598 (1987).
[25] H.G. Bohlen, W. Bohne, B. Gebauer, W. von Oertzen, M. Goldschmidt, H. Hafner, L. Pflug, and K. Wannebo, Phys. Rev. Lett. **37**, 195 (1976).
[26] W.D.M. Rae, N.S. Godwin, D. Sinclair, H.S. Bradlow, P.S. Fisher, J.D. King, A.A. Pilt, and G. Proudfoot, Nucl. Phys. **A319**, 239 (1979).
[27] H.G. Bohlen (unpublished).
[28] H.G. Bohlen (unpublished).
[29] A.M. Lane and R.G. Thomas, Rev. Mod. Phys. **30**, 257 (1958).
[30] E. Byckling and K. Kajantie, *Particle Kinematics* (Wiley, London, 1973).